

Developing flexible liquid crystal defect mode lasers

Taimoor Ali*, Jia-De Lin, Yuping Shi, Steve J. Elston, and Stephen M. Morris*
Department of Engineering Science, University of Oxford, Parks Road, Oxford, OX1 3PJ, UK

ABSTRACT

The challenges associated with developing a flexible defect-mode liquid crystal (LC) laser are addressed in this paper. To begin with, we discuss the process for creating a well-aligned photopolymerized film of chiral nematic LC using various surface alignment layers such as polyvinyl alcohol, sulphonic azo-dye and rubbed polyimide. A single mode flexible defect-mode laser is demonstrated with an excitation threshold fluence of $60\mu\text{J}/\text{cm}^2/\text{pulse}$. In accordance with previous studies, results from simulations based on the 4×4 Berreman model show that the wavelength and the number of laser modes are determined by the thickness of the defect layer. The proposed flexible laser can be used to form lasers that can be integrated into conformable platforms and that can be used to control the beam direction without the need for additional optical components.

Keywords: Liquid crystal, solution processing, flexible laser, defect-mode laser, thin-film lasers, wearable technology

1. INTRODUCTION

1.1 Defect-modes in chiral nematic LCs

It is well known that liquid crystals (LC) exhibit optical anisotropy and the most commonly studied LC phase is the nematic phase. Figure 1(a) shows the optical indicatrix with refractive indices along the three principal axes relative to the optic axis. When a nematic LC is doped with a chiral dopant, the molecules spontaneously self-organise to form a helical structure, as shown in Figure 1(b). This is known as chiral nematic LC phase. The distance over which the director rotates through an angle of 2π to form the helical structure is referred to as the pitch (p)^{1,2}.

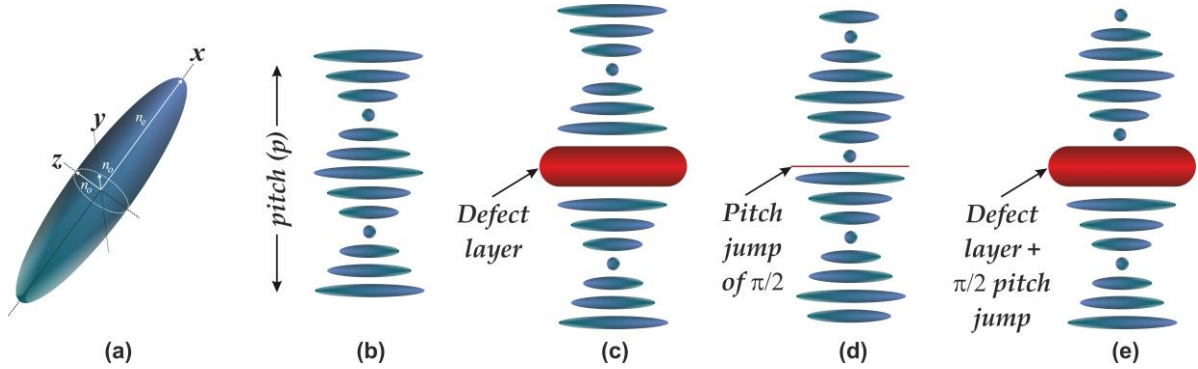


Figure 1: (a) The optical indicatrix with the corresponding refractive indices, (b) a chiral nematic LC, (c) an isotropic defect layer in the helix, (d) a defect plane creating a pitch jump within the helix, and (e) a combination of c & d.

The pitch is an important parameter in the chiral nematic LC phase since, along with the refractive indices, it determines the wavelength and width of the photonic band gap (PBG). Depending upon the handedness of the chiral dopant, the helical structure can be either left- or right-handed. When the chiral nematic LC is illuminated with circularly polarized white light that matches the handedness of the helix and that is of the order of the pitch of the helix, the incident light is reflected. This reflection band can be easily observed in the transmission spectrum as a dip in the spectrum is seen^{3,4}. The short-wavelength and long-wavelength edges of the band-gap are defined by

$$\lambda_s = n_o p \quad (1)$$

*taimoor.ali@eng.ox.ac.uk, stephen.morris@eng.ox.ac.uk

and

$$\lambda_L = n_e p \quad (2)$$

respectively. Here p is the pitch of helix, n_o and n_e are the ordinary and extraordinary refractive indices of the LC, respectively, λ_s and λ_L are the short and long-wavelength edges of the PBG, respectively. Equations 1 & 2 demonstrate that the PBG can be positioned anywhere in the visible spectrum by changing either the birefringence or the pitch of the helix. For a chiral nematic, the pitch can be adjusted by varying the concentration of the chiral dopant and obeys the relationship

$$p = [c\beta]^{-1} \quad (3)$$

where c is the concentration and HTP is the helical twisting power of the chiral dopant, respectively.

The self-organization of the periodic structure is a particularly attractive feature as it represents a facile means of preparing a material with a PBG for visible light. This periodic structure can also act as a laser cavity⁵⁻⁷ when a gain medium is added to the LC such as a laser dye^{8,9}. Laser emission in such structures can occur at the edges of the band-gap when the fluorescence from the laser dye overlaps with one of the edges of the gap: as a result, these are known as band-edge lasers¹⁰. While such lasers can be readily formed by mixing an LC host with a gain medium, the two have to be compatible, which limits the choice of gain medium. For example, advanced functional materials such as quantum dots¹¹⁻¹³, nanocrystals¹⁴ and perovskite¹⁵ tend to aggregate in LC hosts without adequate surface passivation. In addition, when dye-doped CLCs are photo-polymerized to form solid thin films, the gain medium can photo-bleach which can lead to a degradation in the laser emission performance such as an increase in the laser threshold¹⁶⁻¹⁹.

As an alternative, it is desirable to separate the gain medium from the CLC structure. This avoids the aggregation of the material in the CLC and unwanted bleaching created when photo-polymerizing. Such an architecture is the defect-mode structure in which the gain medium is sandwich between two identical CLC reflectors²⁰⁻²⁴.

1.2 Defect-mode structure

A defect structure is formed when a discontinuity is introduced into the CLC helix either by adding an isotropic layer, or by introducing a pitch jump within the helix, or by a combination of the two^{4,25}. This is shown in the Figure 1 (c) – (e). In the current study, the defect structure is formed by inserting an isotropic layer between two identical CLC reflectors, as shown in Figure 2(a). As the neat CLC exhibits a PBG, i.e., forbidden band for visible light, when the defect structure is formed, this discontinuity in the CLC helix creates one or more localized leaky modes within the gap from where light can escape. These leaky mode(s) are created by adding a defect in the helix and are therefore known as defect-modes²⁶⁻²⁸. When the defect layer is doped with an emissive material that exhibits photoluminescence (PL) emission so that the spectrum overlaps with the leaky mode(s), laser emission can be observed. In this regard, the relative position of the leaky modes in the gap to the PL spectrum of the gain medium is crucial for defect-mode laser emission, as shown in Figure 2 (b).

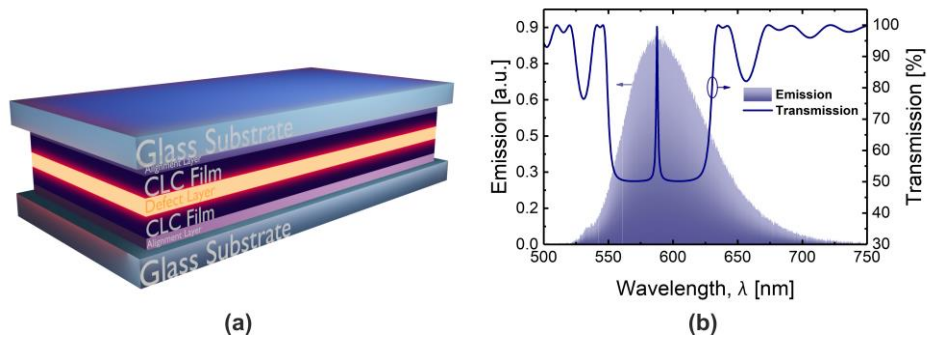


Figure 2: (a) The device architecture of a defect mode structure consists, and (b) the position of the defect mode in PBG with respect to the photoluminescence spectrum of the gain medium.

1.3 Solution processed thin-film lasers

Over the past few decades, solution processed thin-film lasers have gained considerable attention due to their versatility and ease-of-fabrication. Solution processing covers a wide range of techniques including spin coating, drop-casting, bar-

coating, dip-coating, spray-coating and screen printing. Unlike conventional inorganic semiconductor device processing, solution processed devices are easy to fabricate and do not require stringent processing conditions. This reduces the device cost and increases the throughput, which potentially enables large scale production using roll-to-roll methods^{29,30}.

Solution processed thin film lasers encompass a wide-range of materials, providing accessibility to wavelengths across the visible and near-infrared electromagnetic spectrum. The use of facile and cost-effective fabrication techniques makes them a potential candidate for a variety of applications including telecommunications, sensors, virtual and augmented reality displays, and biomedical point-of-care devices. With the use of flexible substrates, it then becomes possible to integrate these thin-film lasers into optical circuits and into technologies that can interact with the human body. Flexible thin-film lasers can potentially also be used in microelectromechanical systems for optomechanical sensing as they can exhibit tuning when they are deformed.

In the current study, a defect-mode structure is formed using photo-polymerized CLC films. This paper addresses the challenges faced in developing a defect-mode laser based upon flexible substrates. The LC materials can form laser cavities on the micron scale without the need for complicated fabrication processes. In this paper, we identify the procedure required for fabricating these defect-mode LC lasers and consider the surface treatment, compatibility of materials and the suitability of flexible substrates. Furthermore, results for single-mode and multi-mode laser emission are demonstrated, and we discuss the experimental techniques employed to avoid the occurrence of the band-edge lasing that might be encountered during the device formation. Lastly, results from simulations are used to demonstrate the possibility of controlling the number and position of the modes in the defect-mode laser.

2. EXPERIMENTS, RESULTS & DISCUSSION

2.1 Device fabrication and characterization

Two photo-polymerizable chiral nematic LC mixtures, obtained from Merck, are used to create the thin film CLC layers. The central wavelengths of the PBG for these mixtures are found to be $\sim 425 \pm 10$ nm and $\sim 615 \pm 10$ nm after photo-polymerization, respectively. In this study, these are designated as Mixture I and Mixture II, respectively. The uncured mixture exhibits a clearing temperature of $79 \pm 1^\circ\text{C}$ and is initially dissolved in toluene to lower its viscosity so that it can be readily spin-coated onto a range of substrates.

Since the chiral LC mixtures exist in liquid form, there are therefore a number of methods that can be used to fabricate a thin film. To begin with, the photo-polymerized chiral mixture is spin-coated onto a range of glass substrates that have different alignment layers. Three different materials are tested as alignment layers: these are polyvinyl alcohol (PVA), sulphonic azo-dye (SD1) and rubbed polyimide (PI).

A PVA solution is prepared in distilled water with 1% wt. concentration of PVA. The mixture is then stirred for 6 – 7 hours at 70°C to form a homogeneous solution. The resultant mixture is poured onto filter paper to stain the undissolved PVA and the filtered PVA solution is drop casted on a clean glass substrate using a pipette before being spin-coated at 1000 rpm for 60 sec. The substrate is then baked in an oven at 90°C for 30 minutes to evaporate any residual water content. After this, the substrate is rubbed with a rubbing machine consisting of rotating a drum covered with clean velvet cloth. The rubbing takes place in one direction for 3 – 5 times. Care is taken while rubbing the substrate along one direction only. Rubbing the PVA-coated substrate promotes a planar alignment of the LC director at the substrate interface. Once the substrate is ready, the photo-polymerized CLC Mixture I is drop-casted and spun-coated at 2000 rpm for 30 sec. The substrate is then baked at 75°C for 60 sec in an oven and then photo-cured with UV radiation (365 nm) at $20 \pm 5 \text{ mW/cm}^2$ for 60 sec. The fabrication steps are illustrated in **Figure 3**.

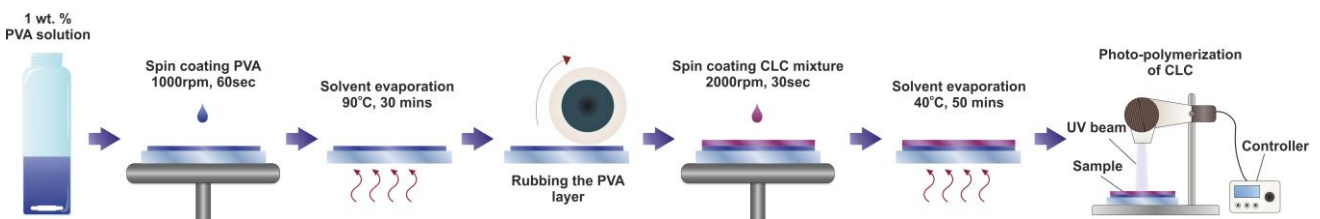


Figure 3: The experimental procedure for creating a PVA-treated substrate for the thin CLC film.

The sample is illuminated with unpolarized white light by placing it in an optical characterization setup as shown in **Figure 4**. The setup includes a white light source that illuminates the LC sample before the emerging light is then collected by a microscope objective and focused onto a fiber that is connected to an Ocean Optics USB 2000+ spectrometer. The transmission spectrum is recorded and shown in **Figure 5(a)**. Even though the sample shows the existence of a band-gap, the quality of the gap is not as expected. Furthermore, the film quality was also inspected on an optical polarization microscope, as shown in Figure 5(b), which shows the appearance of defects and non-uniformity in the alignment in accordance with the poor reflection quality of the film.



Figure 4: The free space optical setup to study the transmission of the thin film of CLC.

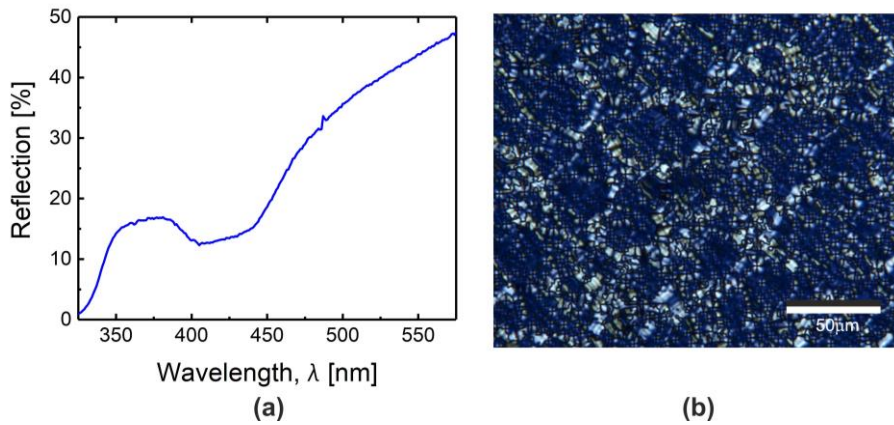


Figure 5: (a) The transmission spectrum, and (b) optical polarization microscope image of a CLC film aligned on the PVA treated substrate.

The second substrate was prepared using the azo-benzene sulphonic dye, commonly referred to as SD1, as an alignment layer on the glass substrate. Initially, SD1 is dissolved into the solvent DMF (N,N-Dimethylformamide) at a 1 mg/ml solution before being spin-coated onto glass at 2000 rpm for 20 seconds. Following this, the SD1-coated substrate was annealed at 110 °C for 10 minutes. Once the SD1 layer was created on the glass substrate, the photo-polymerized CLC Mixture I was spin-coated at 2000 rpm for 30 sec, baked at 40 °C for 50 minutes and then photo-cured using UV radiation (365 nm) at a power density of 20 ± 5 mW/cm² for 60 sec. The fabrication process is shown in **Figure 6**. The CLC film was then placed on the optical setup as shown in Figure 4. The transmission spectrum that was recorded is illustrated in **Figure 7(a)**, this again forms a CLC film with a poor reflection spectrum, indicating a non-uniform alignment of the helical structure. The film quality was studied on an optical polarization microscope as shown in Figure 7(b). Again, defects appear and the film is non-uniform as expected from the transmission spectrum.

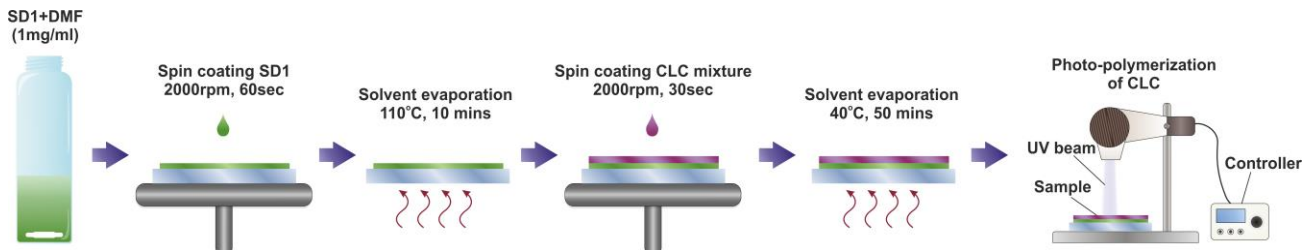


Figure 6: The fabrication steps used in this study to create an SD1-treated substrate and the preparation of the CLC film.

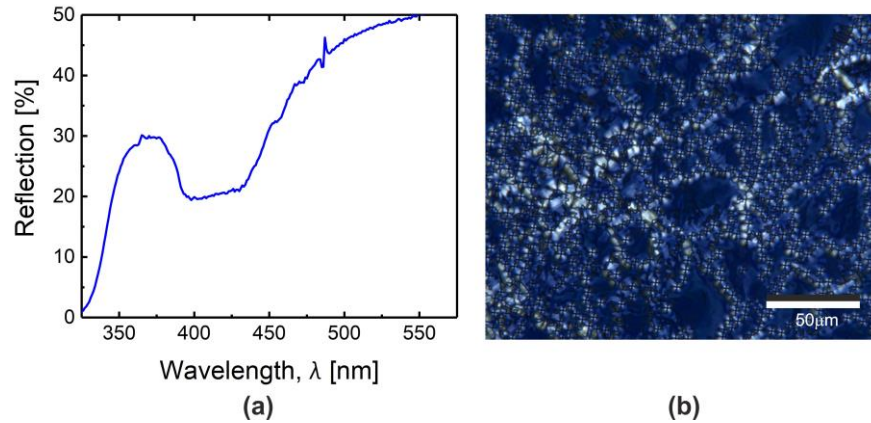


Figure 7: (a) The transmission spectrum, and (b) optical polarization microscope image of a CLC film created on the SD1 treated substrate.

The third type of substrate considered in this study was prepared using a commercially available planar-aligned cell that consisted of rubbed polyimide (PI) as an alignment layer. The glass substrates of the cell were separated to yield two identical glass substrates with PI layers. The photo-polymerized CLC Mixture I was then spin-coated at 2000 rpm for 30 sec, baked at 40 °C for 50 minutes and photo-cured with UV radiation at a wavelength of 365 nm at a power density of $20 \pm 5 \text{ mW/cm}^2$ for 60 sec. The fabrication steps are illustrated in **Figure 8**. The resultant CLC film was then illuminated with white light using the optical setup shown in Figure 4. The transmission spectrum also shows a low reflection quality as shown in **Figure 9(a)**. Again, the film consists of several defects and non-uniformities as seen when the sample is observed on an optical polarization microscope, as shown in Figure 9(b).

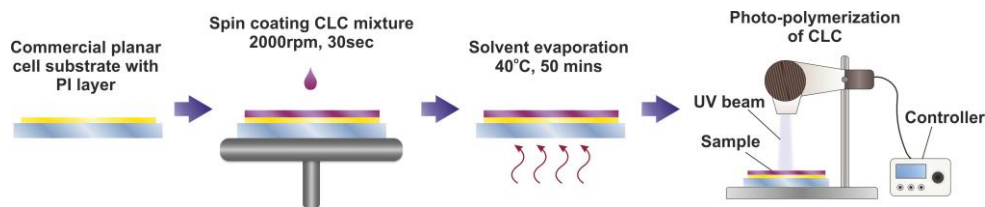


Figure 8: The experimental steps for creating a thin film of CLC on a PI-treated commercial planar substrate.

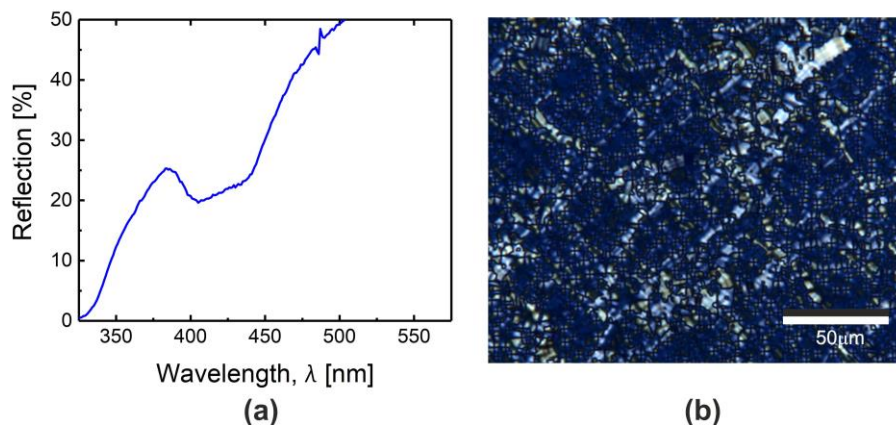


Figure 9: (a) The transmission spectrum, and (b) optical polarization microscope image of a CLC film created on the PI treated commercial substrate.

In the last type consisted, a commercially available 5 μm planar cell was used. The cell consists of the rubbed PI layer as an alignment layer. The empty cell was heated to 80 °C, which is above the clearing temperature of the chiral mixture.

Mixture II was used to create a photo-polymerized CLC film. The toluene solvent, in which the CLC was dispersed, was first evaporated by stirring the mixture at room temperature ($T = 25\text{ }^{\circ}\text{C}$) for 40 hours at 200 rpm and then the photo-polymerized chiral mixture was injected into the cell. Due to heating, the mixture becomes less viscous and fills the cell via capillary action. Once filled, the cell was cooled down to room temperature. The cell was left on a flat surface in dark conditions for 48 hours and then inspected on an optical microscope with a long pass filter to block UV wavelengths and prevent unwanted polymerization. After confirming that the sample consisted of a low number of disclination lines, the cell was photocured on one side using UV (365 nm) radiation with a power density of $40\pm 5\text{ mW/cm}^2$ for 15 secs. After photo-polymerization, the cell was delaminated and the superstrate was removed; this exposed the photo-polymerized CLC thin film.

After removal from the glass cell, the photo-polymerized CLC film had to be transferred to a flexible substrate. To achieve this, the CLC film and underlying glass substrate was immersed into either acetone or isopropyl alcohol (IPA) to release the CLC film from the glass substrate. When the CLC film was immersed in acetone, it was found that it started to damage the film within a few minutes. However, IPA did not show any negative effect on the film even after 48 hours.

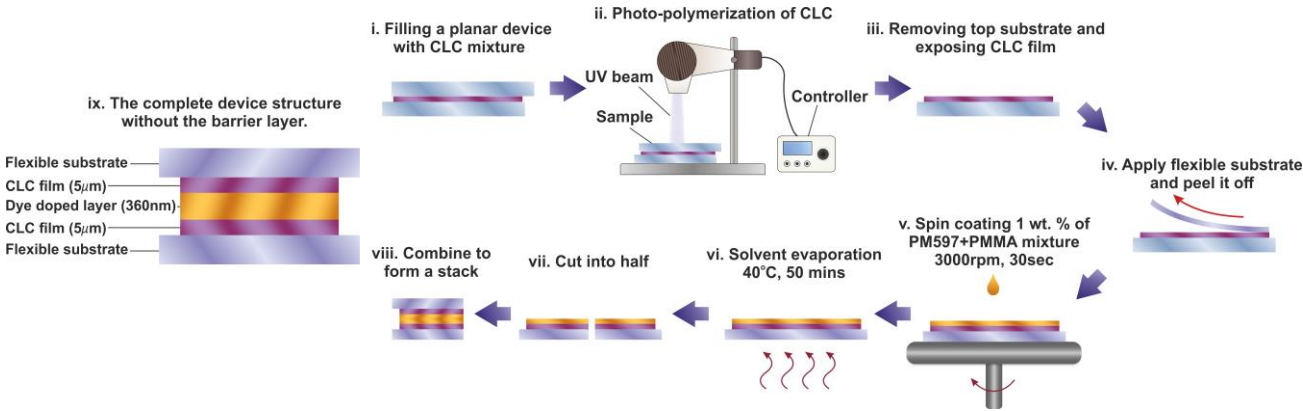


Figure 10. Fabrication steps for creating the flexible defect-mode laser with no barrier layer.

A transparent flexible pressure sensitive adhesive substrate was then applied to the exposed CLC/glass substrate stack and the flexible substrate was gently rubbed in one direction. The flexible substrate was slowly peeled-off from the glass substrate which transferred the photo-polymerized CLC to the flexible substrate. The complete fabrication process is shown in **Figure 10**. After transferring the CLC film onto the flexible substrate, the defect layer consisting of the gain medium was spin-coated at 4000 rpm for 30 secs. The gain medium comprises 1 wt. % of laser dye, PM597, dispersed in Polymethyl methacrylate (PMMA) and anisole. The CLC and gain medium stack was then heated to $40\text{ }^{\circ}\text{C}$ for 50 minutes so as to evaporate the anisole. Finally, a second, identical CLC film attached to a flexible substrate was applied on top of the gain medium layer to form a defect structure comprising a flexible substrate/CLC/gain medium layer/CLC/flexible substrate, as shown in Figure 10.

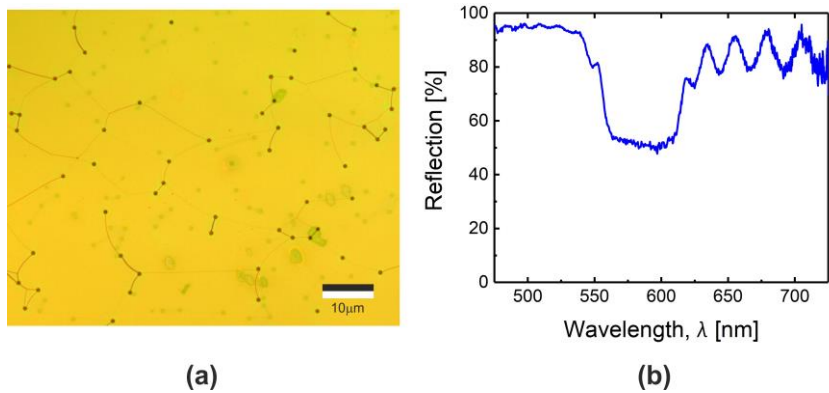


Figure 11: (a) The transmission spectrum, and (b) optical polarization microscope image of a CLC film created on the commercial planar cell.

The film quality and the reflection band was then again studied. The optical polarization microscope images (**Figure 11(a)**) reveals that the CLC film has a uniform area with few disclination lines. This is expected from a well-aligned uniform standing helix configuration. Furthermore, the transmission spectrum of the film was studied using the optical setup and the result is presented in Figure 11(b). The transmission spectrum suggests that the CLC film created with this method forms a much more uniform standing helix configuration with the helix axis normal to the substrate. The reflection band is found to be centered at 585 nm, which is slightly blue-shifted from the expected value and is likely due to the contraction of the film as a result of the evaporation of the host material in which the PMMA was dissolved.

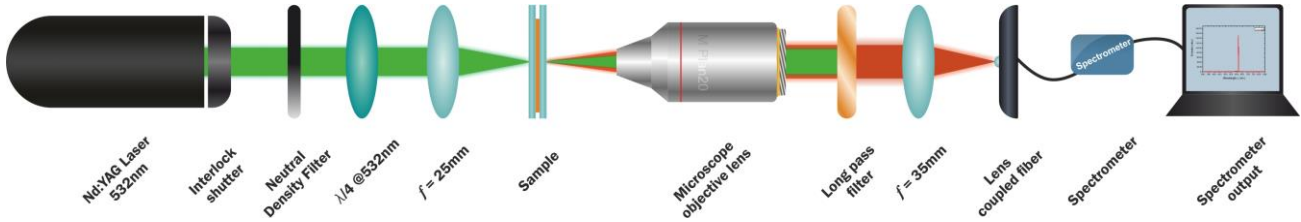


Figure 12: The free space optical setup for optically exciting the samples using a nanosecond Nd:YAG (532 nm) pump laser.

The complete device stack was optically pumped with a nanosecond pulsed Nd:YAG laser emitting at the second harmonic of 532 nm. The free space optical setup is shown in **Figure 12**. The microscope objective ensures that the highly divergent laser emission is captured from the sample and is directed to the optical fiber that is connected to the spectrometer. The long-pass filter between the entrance of the optical fiber and the microscope objective cuts out the pump laser to avoid saturation of the spectrometer. When the CLC stack is optically pumped, multimode laser emission is observed, as shown in **Figure 13**. This is because laser emission occurs both within the band-gap as well as at the edges of the gap. Band-edge laser emission can result due to the penetration of a small concentration of the laser dye into the bare CLC reflectors. Laser emission that occurs within the band-gap, however, is due to the defect-mode structure.

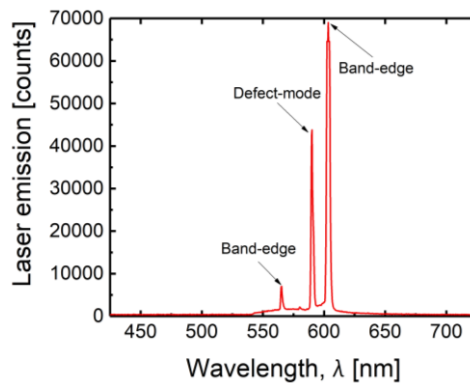


Figure 13: Band-edge and defect-mode laser emission from the flexible, but unprotected CLC film.

Band-edge laser emission in this case is undesirable and in order to avoid the emission at the edges, a barrier layer is needed to protect the CLC film. This barrier layer can prevent the dye from penetrating into the CLC polymer network. A solution of PMMA/anisole was used as a barrier layer. The solution was spin-coated onto the neat CLC film attached to the flexible substrate at 4000 rpm for 30 sec. The sample was then heated to 40 °C for 50 minutes to evaporate the solvent and to form a solid layer of PMMA. This barrier layer of neat PMMA was employed to stop the dye from penetrating into the CLC film when the dye-doped PMMA solution was deposited. After adding the gain medium, defect-mode layer onto the barrier layer, a second CLC/PMMA film on a flexible substrate was then attached on the top of the gain medium layer thereby forming a complete stack of flexible substrate / CLC / PMMA / PMMA+dye / PMMA / CLC / flexible substrate. The fabrication steps are illustrated in **Figure 14**.

Once the complete device stack had been fabricated, it was optically excited with the Nd:YAG laser (532nm). The emission spectrum is presented in **Figure 15**. In this case, the device shows no laser emission at the edges of the band-gap, suggesting that the barrier layer has protected the CLC films from the gain medium layer. The laser exhibits single mode emission that is centered at $\lambda_c = 578.5$ nm.

The position of the laser mode is important and is dependent on the physical parameters such as thickness and refractive index of the defect layer. The spin coating parameters used to create the defect layer of 670 ± 10 nm thick layer. This includes 180 ± 5 nm for each of the barrier layers and 310 ± 5 nm for defect layer which includes the dye.

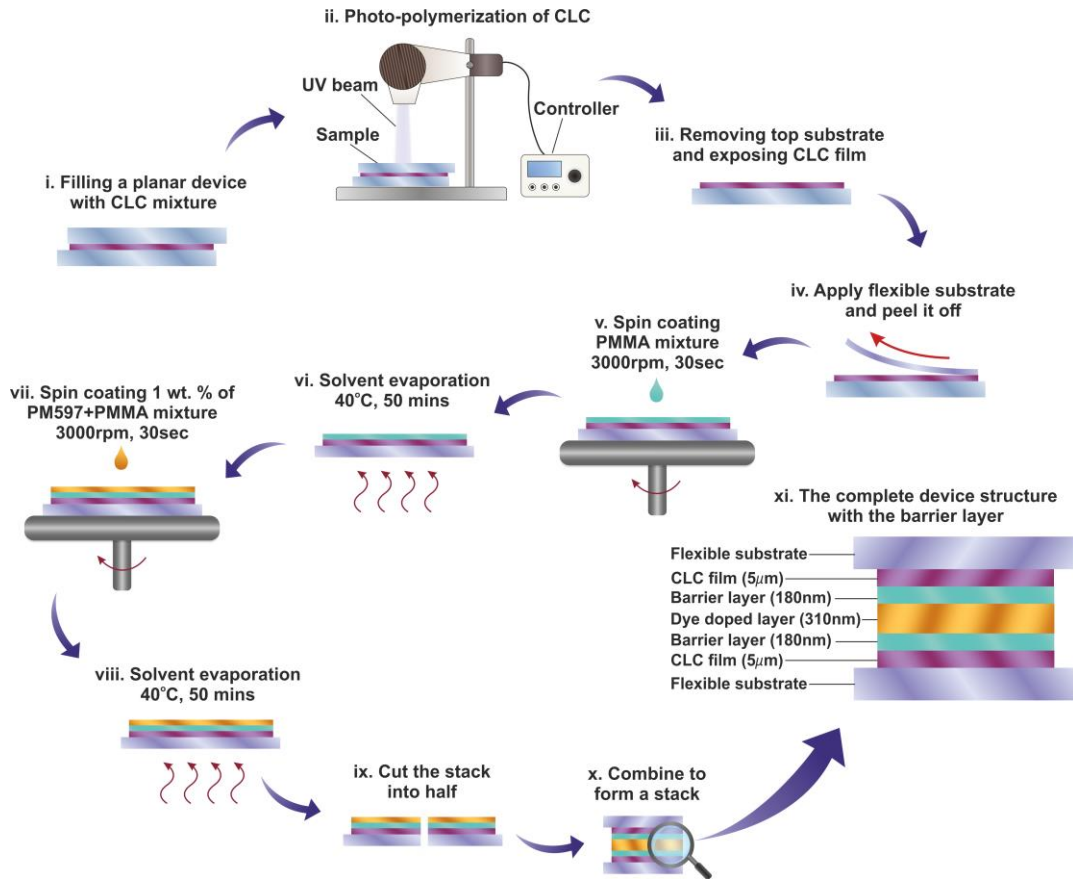


Figure 14: Fabrication steps for creating a flexible defect-mode laser with a barrier layer (i) injecting photo-polymerized CLC mixture into a LC cell with planar alignment, (ii) photo-polymerizing the CLC mixture using UV (365nm) light to create a thin film, (iii) delaminating the top substrate to expose the CLC film, (iv) apply the flexible substrate onto the CLC and carefully transferring the CLC film, (v) spin-coat PMMA/anisole mixture to create a barrier layer, (vi) evaporation of anisole, (vii) spin-coat the dye-doped PMMA/anisole solution, (viii) evaporation of anisole, (ix) cutting stack into two (x) combining the two stacks and (xi) the complete device stack.

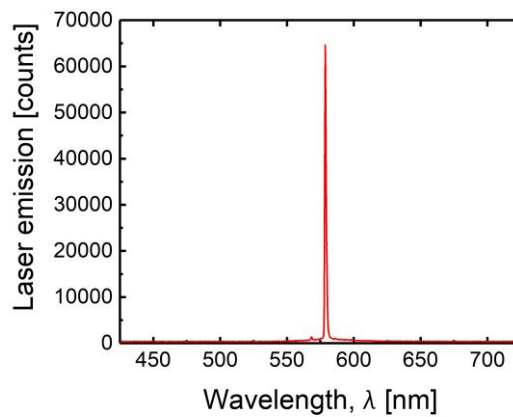


Figure 15: The single mode lasing emission from thin film flexible laser with the barrier layer.

The threshold fluence was determined by varying the pump energy and the corresponding LC laser intensity was then recorded. The variation in pump energy with respect to the output laser intensity is plotted in **Figure 16**. The laser threshold is taken to be the point where the slope of the input-output characteristics changes abruptly. In this case, the laser threshold is recorded to be $60 \mu\text{J}/\text{cm}^2/\text{pulse}$, which is lower than previously reported LC band-edge or defect-mode lasers³¹⁻³⁷. In general, the defect-mode configuration exhibits lower threshold fluence compared to the band edge configuration due to the larger density of states located at the defect-mode⁵. It is believed that the lower threshold in the proposed device is a result of the high quantum efficiency ($>70\%$) of the PM579 laser dye³⁸. Furthermore, we recently demonstrated a flexible defect-mode laser with an excitation fluence of $12.3 \mu\text{J}/\text{cm}^2/\text{pulse}$ ³⁹. However, for the device presented in this paper the slight increase in the threshold fluence is considered to be the result of lower quality film formation, which leads to nonuniform interfaces that give rise to light scattering and therefore greater cavity losses.

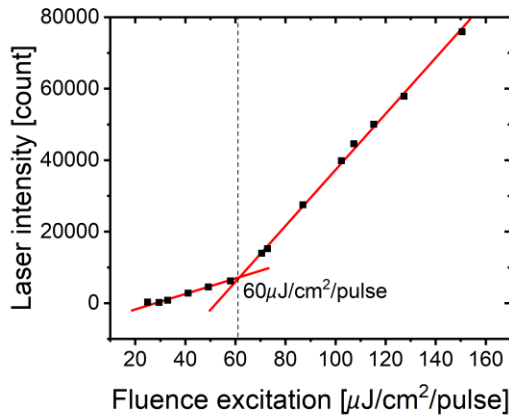


Figure 16: The laser intensity as a function of excitation fluence to determine the threshold of the flexible laser.

By varying the processing parameters, a thicker defect layer was also deposited, which could, in principle, support multimode laser emission. This is shown in **Figure 17** consisting of laser emission at two different wavelengths i.e., 575 nm and 586 nm. The presence of multimodes in a defect-mode structure is also demonstrated using 4×4 Berreman simulations in the next section.

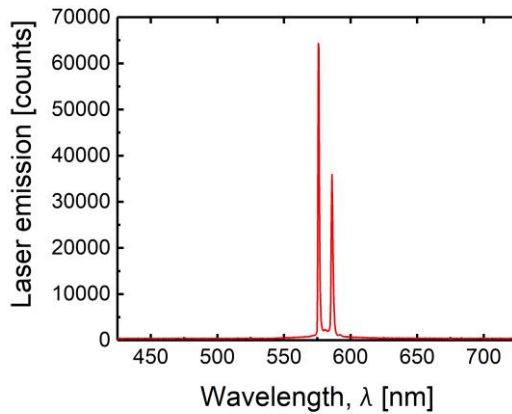


Figure 17: The multimode laser emission from the thick defect layer structure.

2.2 4×4 Berreman model simulation

The number of laser modes and their corresponding wavelength within the band-gap depends on the thickness and refractive index of the defect layer. A thick layer can support multimodes within the gap; however, a thin defect-mode layer can support at least a single mode. 4×4 Berreman simulations were performed with the same device parameters used in the experiment. In the simulations, defect layer parameters such as thickness and refractive index were set to 670

nm and 1.50, respectively. On the other hand, each CLC film had a thickness of 5026 nm, pitch 359 nm and $n_o = 1.56$ and $n_e = 1.67$. The transmission spectrum from the simulation is shown in **Figure 18**. The result suggests that the position of the laser mode corresponds to the single mode laser emission as seen in Figure 15. This also confirms that the laser is a result of the defect-mode structure.

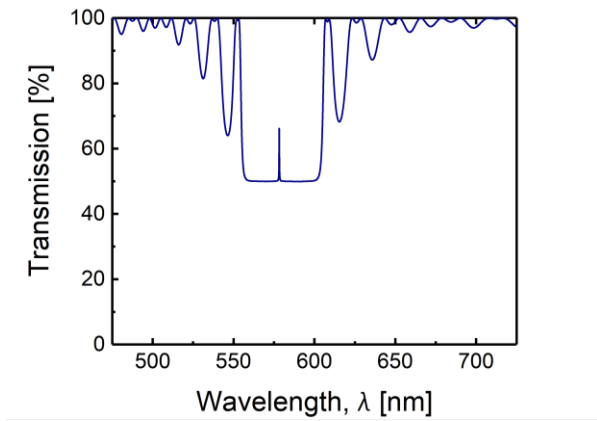


Figure 18: Simulations of the transmission spectrum using the 4×4 Berreman model, which shows a single mode in the gap.

Since the position of the laser emission in the defect-mode is sensitive to the thickness of the defect-layer, simulations were run to demonstrate the variation in the wavelength of the mode, and this is illustrated in **Figure 19**. Figure 19 (a) – 19 (c) represents when the defect thickness is varied up to a few hundreds of nanometers: in this case it produces a single mode with a wavelength that changes with the defect thickness. These simulations were run for a thickness of CLC layer equal to 5376 nm, pitch = 384, $n_o = 1.56$ and $n_e = 1.67$.

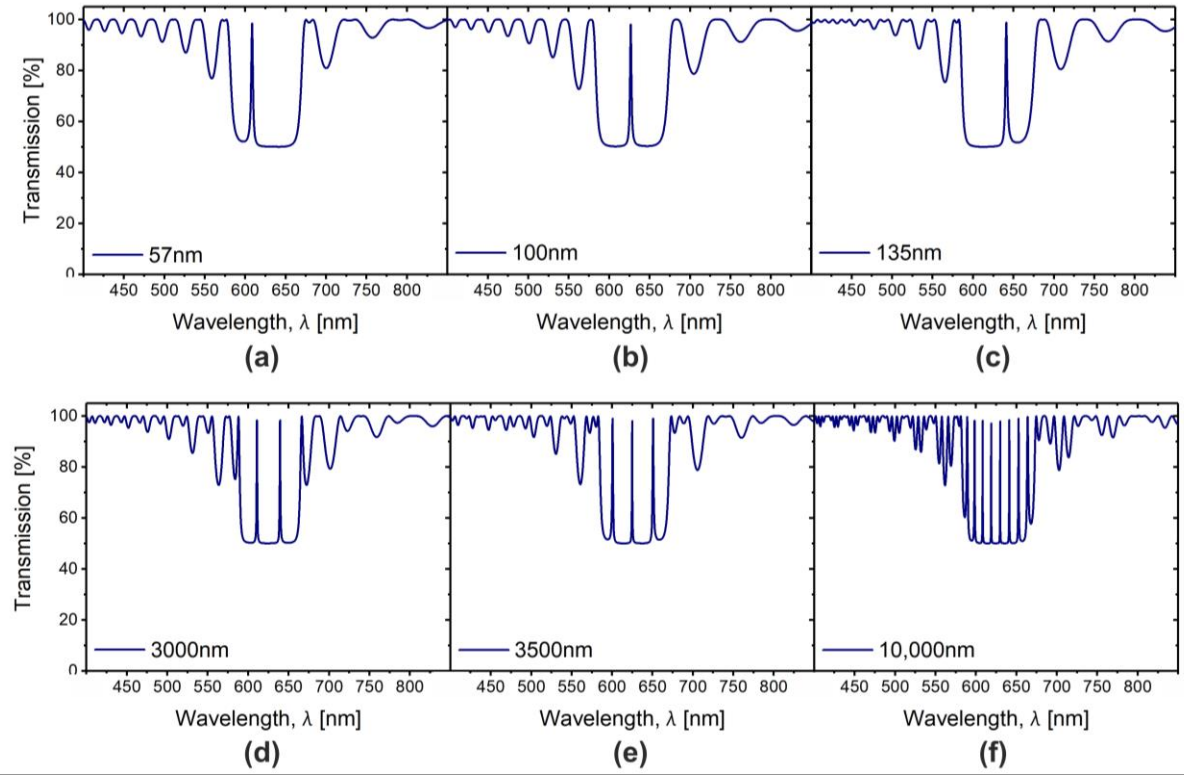


Figure 19: (a – c) The variation in the wavelength of the single mode in the defect mode structure when the thickness of the defect layer is changed, and (d – e) the appearance of multiple modes in the band-gap when the thick defect layer is increased.

When the defect thickness was set to 57 nm, a resonant mode is seen at 608 nm, as shown in Figure 19 (a). However, with a small variation in the thickness of the defect layer i.e., from 57 nm to 135 nm, this single mode is found to red-shift to 641 nm as shown in Figure 19 (c). A contour plot in **Figure 20** (a) highlights the variation in the wavelength of a single mode within the band-gap when the thickness of the defect layer was increased from 10 nm to 200 nm.

Multiple resonant modes can also be observed when the thickness of the defect layer is further increased. Figure 19 (d) – 19 (f) illustrates results from 4×4 Berreman simulations showing the presence of multimodes in the defect-mode structure. Figure 19 (d) shows two modes centered at 610 nm and 639 nm when the thickness of the defect layer is set to 3000 nm. Three resonant modes appear (600 nm, 624 nm and 650 nm) when the thickness is increased to 3500 nm as shown in Figure 19 (e). Further increasing the thickness of the defect layer up to 10,000 nm adds yet more, as illustrated in Figure 19 (f).

Figure 20 (b) is a contour plot that shows the variation in the number of modes in the defect-mode structure when the thickness of the defect layer is changed from 1000 nm to 20,000 nm while keeping other parameters such as the refractive index of the defect layer unchanged.

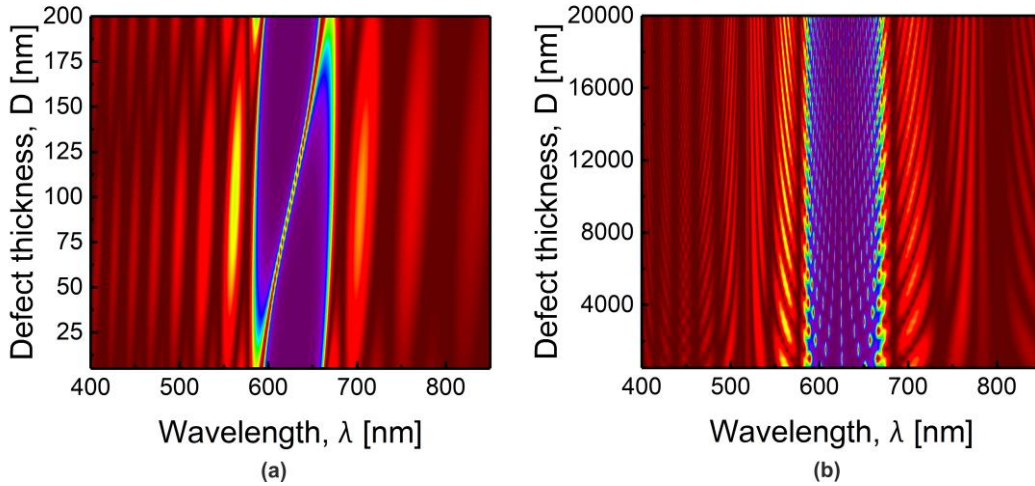


Figure 20: Contour plot shows (a) the variation in the wavelength of the single when the defect layer is varied between 10 nm to 200 nm, and (b) appearance of multimodes within the band-gap by for relatively thick defect layers from 1000nm to 20,000 nm.

3. CONCLUSION

A flexible defect-mode thin-film laser is demonstrated. Results are presented that highlight the challenges in fabricating a flexible defect-modes laser, such as the effect of different types of alignment layer on the formation of the photo-polymerized CLC layers. The experimental procedure employed to minimize the penetration of the gain medium into the polymerized CLC is also discussed. Both single mode and multimode laser emission are demonstrated with the flexible defect-mode laser. The laser threshold from the single mode flexible laser in this study is determined to be $60 \mu\text{J}/\text{cm}^2/\text{pulse}$. The experimental results are supported with simulations using the 4×4 Berreman model, which shows that the number modes in the defect-mode structure is controlled by changing the defect layer thickness. The simulation models are also presented for the experimentally realized device that supports single as well as multimodes. In conclusion, a simple and cost-effective solution processing approach is proposed to create a flexible defect-mode. Due to the mechanical flexibility of the laser, the demonstrated device can could potentially be integrated into wearable and conformable technologies.

REFERENCES

- [1] Collings, P. J. and Hird, M., [Introduction to liquid crystals: Chemistry and physics], CRC Press (2017).
- [2] Elston, S. J., [The Optics of Thermotropic Liquid Crystals], CRC Press (2014).
- [3] Belyakov, V. A., Dmitrienko, V. E. and Orlov, V. P., "Optics of cholesteric liquid crystals," *Sov. Phys. Uspekhi* **22**(2), 64–88 (1979).
- [4] de Vries, H., "Rotatory power and other optical properties of certain liquid crystals," *Acta Crystallogr.* **4**(3), 219–226 (1951).
- [5] Coles, H. and Morris, S., "Liquid-crystal lasers," *Nat. Photonics* **4**(10), 676–685 (2010).
- [6] Folcia, C. L., Ortega, J. and Etxebarria, J., "Cone-Shaped Emissions in Cholesteric Liquid Crystal Lasers: The Role of Anomalous Scattering in Photonic Structures," *ACS Photonics* **5**(11), 4545–4553 (2018).
- [7] Ford, A. D., Morris, S. M. and Coles, H. J., "Photonics and lasing in liquid crystals," *Mater. Today* **9**(7–8), 36–42 (2006).
- [8] Lee, C.-R., Lin, J.-D., Mo, T.-S., Horng, C.-T., Sun, H.-Y. and Huang, S.-Y., "Performance evolution of color cone lasing emissions in dye-doped cholesteric liquid crystals at different fabrication conditions," *Opt. Express* **23**(8), 10168 (2015).
- [9] Schmidtke, J. and Stille, W., "Fluorescence of a dye-doped cholesteric liquid crystal film in the region of the stop band: theory and experiment," *Eur. Phys. J. B - Condens. Matter* **31**(2), 179–194 (2003).
- [10] Dowling, J. P., Scalora, M., Bloemer, M. J. and Bowden, C. M., "The photonic band edge laser: A new approach to gain enhancement," *J. Appl. Phys.* **75**(4), 1896–1899 (1994).
- [11] Chen, L.-J., Lin, J.-D., Huang, S.-Y., Mo, T.-S. and Lee, C.-R., "Thermally and Electrically Tunable Lasing Emission and Amplified Spontaneous Emission in a Composite of Inorganic Quantum Dot Nanocrystals and Organic Cholesteric Liquid Crystals," *Adv. Opt. Mater.* **1**(9), 637–643 (2013).
- [12] Rodarte, A., Cisneros, F., Hein, J., Ghosh, S. and Hirst, L., "Quantum Dot/Liquid Crystal Nanocomposites in Photonic Devices," *Photonics* **2**(3), 855–864 (2015).
- [13] Chen, L.-J., Lin, J.-D. and Lee, C.-R., "An optically stable and tunable quantum dot nanocrystal-embedded cholesteric liquid crystal composite laser," *J. Mater. Chem. C* **2**(22), 4388–4394 (2014).
- [14] Chen, L.-J., Dai, J.-H., Lin, J.-D., Mo, T.-S., Lin, H.-P., Yeh, H.-C., Chuang, Y.-C., Jiang, S.-A. and Lee, C.-R., "Wavelength-Tunable and Highly Stable Perovskite-Quantum-Dot-Doped Lasers with Liquid Crystal Lasing Cavities," research-article, *ACS Appl. Mater. Interfaces* **10**(39), 33307–33315 (2018).
- [15] Wood, S. M., Prévôt, M., Amela-Cortes, M., Cordier, S., Elston, S. J., Molard, Y. and Morris, S. M., "Polarized Phosphorescence of Isotropic and Metal-Based Clustomesogens Dispersed into Chiral Nematic Liquid Crystalline Films," *Adv. Opt. Mater.* **3**(10), 1368–1372 (2015).
- [16] Matsui, T., Ozaki, R., Funamoto, K., Ozaki, M. and Yoshino, K., "Flexible mirrorless laser based on a free-standing film of photopolymerized cholesteric liquid crystal," *Appl. Phys. Lett.* **81**(20), 3741–3743 (2002).
- [17] Finkelmann, H., Kim, S. T., Muñoz, A., Palfy-Muhoray, P. and Taheri, B., "Tunable Mirrorless Lasing in Cholesteric Liquid Crystalline Elastomers," *Adv. Mater.* **13**(14), 1069–1072 (2001).
- [18] Varanytsia, A., Nagai, H., Urayama, K. and Palfy-Muhoray, P., "Tunable lasing in cholesteric liquid crystal elastomers with accurate measurements of strain," *Sci. Rep.* **5**(1), 17739 (2015).
- [19] Shibaev, P. V., Madsen, J. and Genack, A. Z., "Lasing and Narrowing of Spontaneous Emission from Responsive Cholesteric Films," *Chem. Mater.* **16**(8), 1397–1399 (2004).
- [20] Painter, O., Lee, R. K., Scherer, A., Yariv, A., O'Brien, J. D., Dapkus, P. D. and Kim, I., [Two-dimensional photonic band-gap defect mode laser] (1999).
- [21] Zhong, K., Liu, L., Xu, X., Hillen, M., Yamada, A., Zhou, X., Verellen, N., Song, K., Van Cleuvenbergen, S., Vallée, R. and Clays, K., "Defect Mode Passband Lasing in Self-Assembled Photonic Crystal," *ACS Photonics* **3**(12), 2330–2337 (2016).
- [22] Li, M., Lai, X., Li, C. and Song, Y., "Recent advantages of colloidal photonic crystals and their applications for luminescence enhancement," *Mater. Today Nano* **6**, 100039 (2019).
- [23] Zhou, W., Liu, S.-C., Ge, X., Zhao, D., Yang, H., Reuterskiold-Hedlund, C. and Hammar, M., "On-Chip Photonic Crystal Surface-Emitting Membrane Lasers," *IEEE J. Sel. Top. Quantum Electron.* **25**(3), 1–11 (2019).
- [24] Huang, J.-C., Hsiao, Y.-C., Lin, Y.-T., Lee, C.-R. and Lee, W., "Electrically switchable organo-inorganic hybrid for a white-light laser source," *Sci. Rep.* **6**(1), 28363 (2016).
- [25] Yoon, J., Lee, W., Caruge, J. M., Bawendi, M., Thomas, E. L., Kooi, S. and Prasad, P. N., "Defect-mode mirrorless lasing in dye-doped organic/inorganic hybrid one-dimensional photonic crystal," *Appl. Phys. Lett.*

88(9), 10–13 (2006).

- [26] Gevorgyan, A. H. and Oganesyanyan, K. B., “Lasing in cholesteric liquid crystal cells with an isotropic defect layer inside,” *Laser Phys. Lett.* **12**(12), 125805 (2015).
- [27] Ilchishin, I. P., Tikhonov, E. A. and Mykytiuk, T. V., “Narrowing the oscillation spectra of a cholesteric liquid crystal laser,” *Mol. Cryst. Liq. Cryst.* **670**(1), 112–118 (2018).
- [28] Liu, Y. S., Lin, H. C. and Xu, H. L., “The Surface Plasmon Resonance Effect on the Defect-Mode Cholesteric Liquid Crystals Doped with Gold Nanoparticles,” *IEEE Photonics J.* **10**(5), 1–7 (2018).
- [29] Collings, P. J. and Hird, M., [Organic Semiconductor Lasers], CRC Press (2017).
- [30] Collings, P. J. and Hird, M., [Organic Micro/Nanoscale Lasers], CRC Press (2017).
- [31] Song, M. H., Park, B., Shin, K.-C., Ohta, T., Tsunoda, Y., Hoshi, H., Takanishi, Y., Ishikawa, K., Watanabe, J., Nishimura, S., Toyooka, T., Zhu, Z., Swager, T. M. and Takezoe, H., “Effect of Phase Retardation on Defect-Mode Lasing in Polymeric Cholesteric Liquid Crystals,” *Adv. Mater.* **16**(910), 779–783 (2004).
- [32] Yoshida, H., Lee, C. H., Matsuhisa, Y., Fujii, A. and Ozaki, M., “Bottom-Up Fabrication of Photonic Defect Structures in Cholesteric Liquid Crystals Based on Laser-Assisted Modification of the Helix,” *Adv. Mater.* **19**(9), 1187–1190 (2007).
- [33] Jeong, S. M., Ha, N. Y., Takanishi, Y., Ishikawa, K., Takezoe, H., Nishimura, S. and Suzuki, G., “Defect mode lasing from a double-layered dye-doped polymeric cholesteric liquid crystal films with a thin rubbed defect layer,” *Appl. Phys. Lett.* **90**(26), 261108 (2007).
- [34] Ozaki, M., Ozaki, R., Matsui, T. and Yoshino, K., “Twist-Defect-Mode Lasing in Photopolymerized Cholesteric Liquid Crystal,” *Jpn. J. Appl. Phys.* **42**(Part 2, No. 5A), L472–L475 (2003).
- [35] Uchimura, M., Watanabe, Y., Araoka, F., Watanabe, J., Takezoe, H. and Konishi, G., “Development of Laser Dyes to Realize Low Threshold in Dye-Doped Cholesteric Liquid Crystal Lasers,” *Adv. Mater.* **22**(40), 4473–4478 (2010).
- [36] Normand, M. C., Chen, P., Can, C. and Hands, P. J. W., “Overcoming repetition rate limitations in liquid crystal laser systems,” *Opt. Express* **26**(20), 26544 (2018).
- [37] Watanabe, Y., Uchimura, M., Araoka, F., Konishi, G., Watanabe, J. and Takezoe, H., “Extremely Low Threshold in a Pyrene-Doped Distributed Feedback Cholesteric Liquid Crystal Laser,” *Appl. Phys. Express* **2**(10), 102501 (2009).
- [38] Mowatt, C., Morris, S. M., Song, M. H., Wilkinson, T. D., Friend, R. H. and Coles, H. J., “Comparison of the performance of photonic band-edge liquid crystal lasers using different dyes as the gain medium,” *J. Appl. Phys.* **107**(4), 043101 (2010).
- [39] Ali, T., Lin, J., Snow, B., Wang, X., Elston, S. J. and Morris, S. M., “A Thin-Film Flexible Defect-Mode Laser,” *Adv. Opt. Mater.*, 1901891 (2020).